Triplet Exciton Activation in Moderately Coupled (0.21 eV), Discrete Tetrakis(methylthio)-TTF$^{\bullet+}$ Dimers: A Manifestation of the Weakening of the Intradimer Interaction upon Binding of the Outer Methylthio and Thiocyanate Functionalities in $[(MeS)_4TTF^{\bullet+}]_2[Mo_6Cl_8(NCS)_6^{2-}]$, Completed by the Synthesis and Structure of the Tetrabutylammonium Salt of the Cluster Dianion, $(Bu_4N)_2[Mo_6Cl_8(NCS)_6]$

Aude Guirauden,[†] Ib Johannsen,[‡] Patrick Batail,*[,†] and Claude Coulon*[,§]

Laboratoire de Physique des Solides Associé au CNRS (URA 02), Université de Paris-Sud, 91405 Orsay, France, and Centre de Recherche Paul Pascal du CNRS, Avenue Dr. Schweitzer, 33600 Pessac, France

Received October 6, 1992

Reaction of $MoCl_2$ with NaOH followed by the addition of $Bu_4N(NCS)$ and HBF_4 in methanol affords $(Bu_4N)_2[Mo_6Cl_8(NCS)_6]$ (**1**), whose crystal structure is reported: space group $P2_1/c$, $Z = 2$, $a = 10.443(6)$ Å, $b = 19.568(3)$ Å, $c = 15.654(2)$ Å, $\beta = 94.20(2)°$, $V = 3190(3)$ Å^3. Single crystals of $[(MeS)_4TTF]_2[Mo_6Cl_8(NCS)_6]$ (**2**) were grown by oxidation of tetrakis(methylthio)tetrathiafulvalene, $(MeS)_4TTF$, in the presence of the tetrabutylammonium salt **1**, and the structure of **2** was determined: space group $P\bar{1}$, $Z = 1$, $a = 11.568(1)$ Å, $b = 13.931(1)$ Å, $c = 11.299(2)$ Å, $\alpha = 93.52(1)°$, $\beta = 110.71(1)°$, $\gamma = 64.03(1)°$, $V = 1521.7(4)$ Å^3. The structure of **2** consists of discrete $[(MeS)_4TTF^{\bullet+}]_2$ dimers with a slipped pattern of overlap of the planar molecular cation radicals. The binding of the dimers and the inorganic cluster anion framework occurs via S···S and C–H···S contacts. The ESR spectrum observed at room temperature is characteristic of mobile triplet Frenkel excitations whose features are thoroughly analyzed. The experimental determination of the fine structure tensor principal values and axes affords the zero-field splitting (ZFS) parameters $D = -315$ G and $E = 35$ G and the tensor orientation, leading to the conclusion that the unpaired electrons in the triplet state (observed and calculated magnetic gaps of 0.211 and 0.215 eV, respectively) remain adjacent within the cation radical dimer. A manifestation of this correlation is found in the close proximity between the fine structure tensor axes and dimer molecular symmetry axes, thereby allowing a unique correlation to be made between the molecular dimer spin density and configuration and the effect of organic–inorganic chalcogen binding in the solid state.

Introduction

The observation of triplet excitons in pairs of organic radicals is the object of recent renewed interest.[1-4] Most of the known examples,[5] summarized in Table I, involve thermally activated triplet spins localized into nonuniform chains or isolated pairs of tetracyanoquinodimethane radical anions, $TCNQ^{\bullet-}$. Here, we report on one such rare[6] example in TTF chemistry. In this new system, the triplet state of discrete, fully oxidized yet moderately coupled dimers of tetrakis(methylthio)tetrathiafulvalenium $(MeS)_4TTF^+$ is thoroughly analyzed and shown to exhibit a fine structure associated with a dissymmetric spin distribution within the centrosymmetric dimers. The pattern of intermolecular association within the structure of the present salt, a consequence of the particular binding of the outer methylthio and thiocyanate functionalities, is shown to be favorable to the activation of a well-defined triplet state. Thus, moderately coupled dimers of planar molecules expressing triplet activity ($S = 1$) have been stabilized in the title compound, in sharp contrast with the occurrence of strongly coupled, eclipsed dimers of distorded tetramethyltetrathiafulvalene molecules in the reference compound[7] $(Me_4TTF^{\bullet+})_2Mo_6Cl_{14}^{2-}$ in which the magnetic gap is too large to exhibit a triplet state. In this respect, the specific binding of the molecular ions in $[(MeS)_4TTF^{\bullet+}]_2[Mo_6Cl_8(NCS)_6^{2-}]$ may be considered to have brought about the dimer triplet exciton activation, exemplifying the sensitivity of the latter to the molecular environment, a concept relevant to the electronic activation of mixed-valence molecular assemblies.[8]

This paper also reports the synthesis[9] of the thiocyanato-functionalized cluster halide as its tetrabutylammonium salt and

[†] Université de Paris-Sud.

[‡] Present address: NKT Research Center, Sognevej 11, DK-2605 Brondby, Denmark.

[§] CRPP-CNRS.

(1) Soos, Z. G. In *Low-Dimensional Cooperative Phenomena*; Keller, H. J., Ed.; NATO ASI Series B; Plenum Press: New York, 1974; p 45.

(2) (a) Grossel, M. C.; Evans, F. A.; Hriljac, J. A.; Morton, J. R.; LePage, Y.; Preston, K. F.; Sutcliffe, L. H.; Williams, A. J. *J. Chem. Soc., Chem. Commun.* **1990**, *439*. (b) Grossel, M. C.; Evans, F. A.; Hriljac, J. A.; Prout, K.; Weston, S. C. *J. Chem. Soc., Chem. Commun.* **1990**, 1494. (c) Hynes, R. C.; Morton, J. R.; Preston, K. F.; Williams, A. J.; Evans, F.; Grossel, M. C.; Sutcliffe, L. H.; Weston, S. C. *J. Chem. Soc., Faraday Trans.* **1991**, *87*, 2229.

(3) Bencini, A.; Zanchini, C. *Inorg. Chem.* **1991**, *30*, 4245.

(4) Reffman, D.; Cornelissen, J. P.; deGraff, R. A.; Haasnoot, J. G.; Reedijk, J. *Inorg. Chem.* **1991**, *30*, 4928.

(5) (a) Jones, M. T.; Chesnut, D. B. *J. Chem. Phys.* **1963**, *38*, 1311. (b) Chesnut, D. B.; Arthur, P., Jr. *J. Chem. Phys.* **1962**, *36*, 2969. (c) Chesnut, D. B.; Phillips, W. D. *J. Chem. Phys.* **1961**, *35*, 1002. (d) Bailey, J. C.; Chesnut, D. B. *J. Chem. Phys.* **1969**, *51*, 5118. (e) Hibma, T.; Sawatzky, G. A.; Kommandeur, J. *Phys. Rev. B* **1977**, *15*, 3959. (f) Flandrois, S.; Choukroun, M. L.; Delhaes, P.; Giuntini, J. C.; Jullien, D.; Zanchetta, J. V. *Mol. Cryst. Liq. Cryst.* **1979**, *52*, 35. (g) Ralph, H. H.; Keller, H. J.; Nöthe, D.; Werner, M.; Gundel, D.; Sixl, H.; Soos, Z. G.; Metzger, R. M. *Mol. Cryst. Liq. Cryst.* **1981**, *65*, 179. (h) Thomas, D. D.; Keller, H.; McConnel, H. M. *J. Chem. Phys.* **1963**, *11*, 2321. (i) Hove, M. J.; Hoffman, B. M.; Ibers, J. A. *J. Chem. Phys.* **1972**, *56*, 3940.

(6) Another example is the observation of the tetrathiafulvalenium dimer triplet state activation above 100 K in $(TTF^{\bullet+})_2[(Nb_6Cl_{18})^{3-}]\cdot[(C_2H_5)_4N^+][CH_3CN]$. In this compound, however, the fine structure is not observed because it is averaged by the collisions between the triplet excitons, which lead to an exchange narrowing of the ESR line in the temperature range of the experiments. Note also that the small value of the activation energy of the exchange narrowing is consistent with the small value of the magnetic gap (see Table I): Pénicaud, A.; Batail, P.; Davidson, P.; Levelut, A. M.; Coulon, C.; Perrin, C. *Chem. Mater.* **1990**, *2*, 117.

(7) Ouahab, L.; Batail, P.; Perrin, C.; Garrigou-Lagrange C. *Mater. Res. Bull.* **1986**, *21*, 1223.

(8) Roberts, J. A.; Hupp, J. T. *Inorg. Chem.* **1992**, *31*, 157.

0020-1669/93/1332-2446$04.00/0 © 1993 American Chemical Society

Table I. Examples of the Reported Triplet Excitons in Cation or Anion Radical Salts Together with the Singlet–Triplet Energy Separation[a]

compound	singlet–triplet energy sepn, eV	ref
Anion Radical Salts		
$[(C_2H_5)_3NH](TCNQ)_2$	0.034	5a
$[(C_6H_5)_3PCH_3](TCNQ)_2$	0.065	5a
$Cs_2(TCNQ)_3$	0.16	5b
(morph)TCNQ	0.41	5c
(morph)TCNQ	0.36	5d
$(morph)_3(TCNQ)_4$	0.33	5d
$(morph)_2(TCNQ)_3$	0.31	5d
RbTCNQ	0.26	5e
(MDCA)TCNQ	0.20 and 0.07[b]	5f
Rb(18-crown-6)TCNQ	0.38	2a
K(18-crown-6)TCNQ	0.37	2b
$Zn(phen)_3(TCNQ)_3$	0.007	3
$(NEP)_2(TCNQ\text{-}TCNQ)$	0.27	5g
Cation Radical Salts		
$(tmpd)ClO_4$	0.03 (45 K)	5h
$(tmpd)_2[Ni(mnt)_2]$	0.24	5i
$(tmpd)_2[Ni(dmit)_2]$	0.22	4
$(TTF)_2(Nb_6Cl_{18})(Et_4N)(CH_3CN)$	0.07	6
$[(MeS)_4TTF]_2[Mo_6Cl_8(NCS)_6]$	0.22	*c*

[a] morph = morpholinium; MDCA = methyldiethylcyclohexylammonium; tmpd = *N,N,N′,N′*-tetramethyl-*p*-phenylenediamine; phen = 1,10-phenanthroline; NEP = *N*-ethylphenazinium; dmit = 2-thioxo-1,3-dithiole-4,5-dithiolate; Me = methyl; Et = ethyl. [b] Before and after the transition. [c] This work.

its first structural characterization as well,[10] showing that the thiocyanato ligands are N-bonded to the molybdenum cluster core in $(Bu_4N)_2[Mo_6Cl_8(NCS)_6]$. Thus, the presence of outer sulfur atoms on the inorganic cluster dianion prompted us to engage it with cation radicals bearing outer chalcogen atoms with the prospect that such outer functionalities would in fact be effective in producing novel patterns for the molecular ions to fulfill the additional expectation[11] of enhanced intermolecular cation–anion electronic interactions.

Experimental Section

Solvents were dried and distilled before use by standard methods. $(MeS)_4TTF$[12] and $MoCl_2$[13] were synthesized as reported in the literature. $Bu_4N(SCN)$ and HBF_4 were purchased from Fluka.

Preparation of $(Bu_4N)_2[Mo_6Cl_8(NCS)_6]$. A 0.5 N NaOH solution was slowly added dropwise to a suspension of $MoCl_2$ (2.0 g, 2 mmol) in 100 mL of H_2O, stirring at 70 °C, until complete dissolution of $MoCl_2$, which requires about 24 mL (12.0 mmol) of NaOH solution (note that the apparition of a marroon coloration indicates the destruction of the $[Mo_6Cl_8]^{4+}$ cluster core; the NaOH addition should then be stopped immediately and the subsequent filtration should proceed promptly). The final solution was quickly filtered off into an EtOH (250 mL) solution of Bu_4NSCN (1.44 g, 47.9 mmol) and HBF_4 (50% in H_2O, 45 mL, 0.36 mol). The mixture was stirred for $^1/_2$ h, and then the orange crystalline solid was isolated, thoroughly washed with water until neutrality of the washing solution, and dried in vacuo. The solid, recrystallized from a 10/1 mixture of MeOH and CH_3CN, gave good-quality orange crystals (2.4 g, 60%) suitable for X-ray analysis. Anal. Calcd for $(Bu_4N)_2[Mo_6Cl_8(NCS)_6]$, $C_{38}H_{72}Cl_8N_8Mo_6S_6$: C, 26.96; H, 4.30; Cl, 16.75; N, 6.62; S, 11.36. Found: C, 26.92; H, 4.27; Cl, 17.05; N, 6.43; S, 11.26.

Crystallization of $[(MeS)_4TTF]_2[Mo_6Cl_8(NCS)_6]$. The donor was recrystallized three times in cyclohexane. The solvents were dried over activated alumina before use. The solutions and electrochemical cells were degassed with argon. Black, shiny platelets, grown at 21 °C under constant-current electrolysis (2–8 μA; J = 3.2–12.7 μA cm^{-2}) at a platinum wire anode of a CH_3CN/1,1,2-trichloroethane (10 mL/20 mL) solution containing the donor (15 mg, 3.2 mmol) and $(Bu_4N)_2[Mo_6Cl_8(NCS)_6]$ (150 mg, 3.0 mmol), were harvested after 15 days to 2 months.

Crystallography. The data collection details for $(Bu_4N)_2[Mo_6Cl_8(NCS)_6]$ (**1**) and $[(MeS)_4\text{-}TTF]_2[Mo_6Cl_8(NCS)_6]$ (**2**) are summarized in Table II. Preliminary oscillation and Weissenberg photographs indicated that compound **1** has monoclinic symmetry. A orange, shiny single crystal of **1** and a black platelike single crystal of **2**, whose sizes were 0.03 × 0.21 × 0.24 and 0.05 × 0.33 × 0.33 mm, respectively, were used to collect intensity data on an Enraf-Nonius CAD-4F diffractometer. Intensity data were corrected for Lorentz and polarization effects. An absorption correction was carried out (empirical ψ-scan) for **1** only. The numbers of total reflections measured were 8043 ($1 \le \theta \le 28°$; $\pm h,+k,+l$) for **1** and 6285 ($1 \le \theta \le 26°$; $+h,\pm k,\pm l$) for **2**, giving respectively 2534 and 3652 independent reflections with $I > 3\sigma(I)$. The structures were solved by direct (**1**) and Patterson (**2**) and difference Fourier methods. They were refined anisotropically by full-matrix least-squares techniques, with hydrogen atoms included in structure factor calculations at ideal positions and not refined for **2**. Owing to the significant disorder of the tetrabutylammonium cation, no attempt was made at introducing the corresponding hydrogen atoms in the refinements. Scattering factors are from the *International Tables for X-ray Crystallography* and all computer programs are from the Enraf-Nonius Structure Determination Package (SDP). The final positional parameters are given in Table III. The atom labelings for the cluster anions in **1** and **2** are given in Figure 1, and the atom labeling for the $(MeS)_4TTF$ molecule in **2** is given in Figure 2.

ESR Measurements. ESR spectra were recorded on a Varian X-band spectrometer operating at 9.3 GHz and equipped with an Oxford ESR 900 helium cryostat.

Table II. Crystallographic Data for **1** and **2**

	compound	
	$(Bu_4N)_2[Mo_6Cl_8(NCS)_6]$	$[(MeS)_4\text{-}TTF]_2[Mo_6Cl_8(NCS)_6]$
chem formula	$C_{38}H_{72}Mo_6Cl_8S_6N_8$	$C_{26}H_{24}Mo_6Cl_8S_{22}N_6$
fw	1692.70	1985.19
cryst system	monoclinic	triclinic
space group (No.)	$P2_1/c$ (14)	$P\bar{1}$ (2)
a, Å	10.443(6)	11.568(1)
b, Å	19.569(3)	13.931(1)
c, Å	15.654(2)	11.299(2)
α, deg		93.52(1)
β, deg	94.20(2)	110.71(1)
γ, deg		64.03(1)
V, Å^3	3190(3)	1521.7(4)
λ, Å	0.710 73	0.710 73
Z	2	1
T, °C	22	22
ρ_{calcd}, g cm^3	1.76	2.17
μ, cm^{-1}	16.787	22.857
$R(F_o)^a$	0.049	0.035
$R_w(F_o^2)^a$	0.062	0.050

[a] $R = \sum(|F_o| - |F_c|)/\sum|F_o|$ and $R_w = [\sum w(|F_o| - |F_c|)^2/\sum|F_o|^2]^{1/2}$ with $w = 4F_o^2/[\sigma^2(I) + (0.07F_o^2)^2]$.

Results

Preparation of $(Bu_4N)_2[Mo_6Cl_8(NCS)_6]$. Molecular hexanuclear halide clusters are usually obtained by excision[14a] of the $[Mo_6X_8]$ core from the nonmolecular solid MoX_2, as recently reviewed by Lee and Holm.[14b] Thus, the outer bridging ligands are easily displaced by polar solvents to give $Mo_6X_{12}(solv)_2$. The

(9) This hexasubstituted derivative of $MoCl_2$ was first reported in the original paper by Sheldon, as its solvated potassium salt, $K_2Mo_6Cl_8(NCS)_6 \cdot 6H_2O$: Sheldon, J. C. *Nature* **1959**, *184*, 1210. While we were completing the present paper, the following report describing a synthesis and preliminary spectroscopic characterization of $(TBA)_2[Mo_6Cl_8)(NCS)_6]$ came to our attention: Preetz, W.; Braack, P.; Harder, K.; Peters, G. *Z. Anorg. Allg. Chem.* **1992**, *612*, 7.

(10) Note that a novel hexasubstituted derivative of this hexanuclear molybdenum cluster halide, $Mo_6Cl_8(triflate)_6^{2-}$, has been recently synthesized and its structure determined: Shriver, D. F. Personal communication, 1991. See also: Johnston, D. H.; Shriver, D. F. *Abstracts of Papers*, 204th National Meeting of the American Chemical Society, Washington, DC, Aug 23–28, 1992; American Chemical Society: Washington, DC, 1992; INOR 61.

(11) Mori, T.; Wu, P.; Imaeda, K.; Enoki, T.; Inokuchi, H.; Saito, G. *Synth. Met.* **1987**, *19*, 545.

(12) Mizuno, M.; Garito, A. F.; Cava, M. P. *J. Chem. Soc., Chem. Commun.* **1978**, 18.

(13) Nannelli, P.; Bloch, B. P. *Inorg. Synth.* **1989**, *2*, 134.

(14) (a) Fergusson, J. E. *Prep. Inorg. React.* **1971**, *7*, 93. (b) Lee, S. C.; Holm, R. H. *Angew. Chem., Int. Ed. Engl.* **1990**, *29*, 840.

Table III. Atomic Coordinates and Equivalent Isotropic Thermal Parameters for $(Bu_4N)_2[Mo_6Cl_8(NCS)_6]$ (**1**) and $[(MeS)_4TTF]_2[Mo_6Cl_8(NCS)_6]$ (**2**)

	x	*y*	*z*	B_{eq},[a] Å		*x*	*y*	*z*	B_{eq},[a] Å
				$(Bu_4N)_2[Mo_6Cl_8(NCS)_6]$					
Mo1	0.0595(1)	0.08492(5)	−0.02921(6)	4.63(2)	C13	0.712(2)	0.633(1)	−0.063(1)	12.1(6)[b]
Mo2	0.1336(1)	−0.04046(5)	−0.05175(6)	4.57(2)	C14	0.810(2)	0.670(1)	−0.111(2)	17.9(9)[b]
Mo3	−0.0997(1)	−0.00351(5)	−0.10226(6)	4.47(2)	C21	0.323(2)	0.648(1)	0.087(1)	10.5(5)[b]
Cl1	0.2765(3)	0.0452(2)	0.0209(2)	5.70(7)	C22	0.281(3)	0.596(2)	0.073(2)	9.1(8)[b,c]
Cl2	0.0888(3)	0.0387(2)	−0.1731(2)	5.48(7)	C222	0.205(4)	0.658(2)	0.122(3)	12(1)[b,c]
Cl3	−0.1644(3)	0.1152(2)	−0.0747(2)	5.63(7)	C23	0.154(2)	0.580(1)	0.147(2)	15.0(8)[b]
Cl4	0.0248(3)	0.1220(2)	0.1182(2)	5.82(7)	C24	0.070(3)	0.544(2)	0.102(2)	20(1)[b]
N1	0.123(1)	0.1825(5)	−0.0672(7)	6.6(3)	C31	0.320(2)	0.732(1)	−0.019(2)	5.6(5)[b,c]
N2	0.2875(9)	−0.0858(5)	−0.1088(6)	5.8(2)	C312	0.325(2)	0.696(1)	−0.077(2)	6.5(6)[b,c]
N3	−0.2126(9)	−0.0058(5)	−0.2200(6)	5.9(2)	C32	0.266(3)	0.678(1)	−0.090(2)	7.1(7)[b,c]
C1	0.140(1)	0.2268(7)	−0.1093(9)	7.5(4)	C322	0.184(3)	0.718(2)	−0.071(2)	8.9(8)[b,c]
C2	0.377(1)	−0.1083(6)	−0.1390(7)	5.0(3)	C33	0.160(2)	0.728(1)	−0.163(1)	11.6(5)[b]
C3	−0.276(1)	−0.0048(6)	−0.2824(7)	4.9(3)	C34	0.124(2)	0.681(1)	−0.222(1)	13.6(7)[b]
S1	0.1695(5)	0.2927(2)	−0.1699(3)	12.3(1)	C41	0.446(2)	0.746(1)	0.122(2)	11.1(7)[b,c]
S2	0.5012(3)	−0.1397(2)	−0.1781(3)	7.2(1)	C412	0.427(3)	0.771(2)	0.038(2)	2.0(6)[b,c]
S3	−0.3621(5)	−0.0016(2)	−0.3705(2)	9.4(1)	C42	0.498(2)	0.803(1)	0.109(1)	9.2(4)[b]
N	0.401(1)	0.6943(5)	0.0309(7)	7.1(3)[b]	C43	0.516(3)	0.854(1)	0.186(2)	13.0(8)[b,c]
C11	0.520(1)	0.6545(8)	0.0147(9)	7.4(3)[b]	C432	0.509(5)	0.867(3)	0.118(3)	6(1)[b,c]
C12	0.607(1)	0.6913(8)	−0.042(1)	8.7(4)[b]	C44	0.559(2)	0.916(1)	0.183(2)	16.1(8)[b]
				$[(MeS)_4TTF]_2[Mo_6Cl_8(NCS)_6]$					
Mo1	0.00736(5)	−0.06476(4)	0.14160(4)	2.89(1)	S5	0.6268(2)	0.6353(1)	0.4214(2)	3.71(4)
Mo2	0.18777(5)	−0.04325(4)	0.07226(4)	2.88(1)	S6	0.2652(1)	0.5900(1)	0.3726(4)	3.49(4)
Mo3	−0.03210(5)	0.12601(4)	0.07461(4)	2.85(1)	S7	0.4972(1)	0.4825(1)	0.2874(2)	3.64(4)
Cl1	−0.2009(1)	0.0978(1)	0.1361(1)	3.76(4)	S8	0.5212(2)	0.9018(1)	0.6391(2)	6.12(5)
Cl2	0.2155(2)	−0.2224(1)	0.1315(1)	3.85(4)	S9	0.7724(2)	0.7699(1)	0.5409(2)	5.39(5)
Cl3	−0.1409(2)	−0.1397(1)	−0.0063(2)	4.08(4)	S10	0.1135(2)	0.4689(1)	0.2246(2)	4.92(5)
Cl4	0.1552(2)	0.0171(1)	0.2728(1)	3.78(4)	S11	0.3812(2)	0.3416(1)	0.1292(2)	4.94(5)
N1	0.0164(5)	−0.1361(4)	0.3074(5)	4.2(1)	C4	0.4742(5)	0.6492(4)	0.4280(5)	3.0(1)
N2	0.4129(5)	−0.1006(4)	0.1577(5)	4.3(1)	C5	0.4179(5)	0.5812(4)	0.3711(6)	3.2(1)
N3	−0.0795(5)	0.2760(4)	0.1554(5)	4.4(1)	C6	0.5291(6)	0.7941(4)	0.5496(6)	3.9(2)
C1	0.0383(5)	−0.1495(5)	0.4101(6)	3.7(1)	C7	0.6356(6)	0.7393(5)	0.5084(6)	3.8(2)
C2	0.4967(7)	−0.1274(5)	0.1526(6)	4.8(2)	C8	0.2568(6)	0.4946(4)	0.2668(6)	3.4(1)
C3	−0.1301(6)	0.3529(5)	0.1800(6)	4.0(2)	C9	0.3639(6)	0.4444(4)	0.2262(5)	3.3(1)
S1	0.0714(2)	−0.1745(2)	0.5611(2)	5.97(5)	C10	0.3609(9)	0.9458(6)	0.6565(9)	7.0(3)
S2	0.6642(3)	−0.1812(3)	0.1483(3)	10.2(1)	C11	0.8809(8)	0.6656(7)	0.474(1)	7.9(3)
S3	−0.2049(2)	0.4709(2)	0.2264(3)	7.66(7)	C12	−0.0207(7)	0.5961(7)	0.1400(9)	6.3(3)
S4	0.3999(2)	0.7521(1)	0.5097(2)	3.81(4)	C13	0.4949(8)	0.3493(7)	0.0602(8)	7.4(3)

[a] $B = (4/3)[a^2B(1,1) + b^2B(2,2) + c^2B(3,3) + ab(\cos\gamma)B(1,2) + ac(\cos\beta)B(1,3) + bc(\cos\alpha)B(2,3)]$. [b] Atoms refined isotropically. [c] Atoms refined with a site occupancy of 0.5.

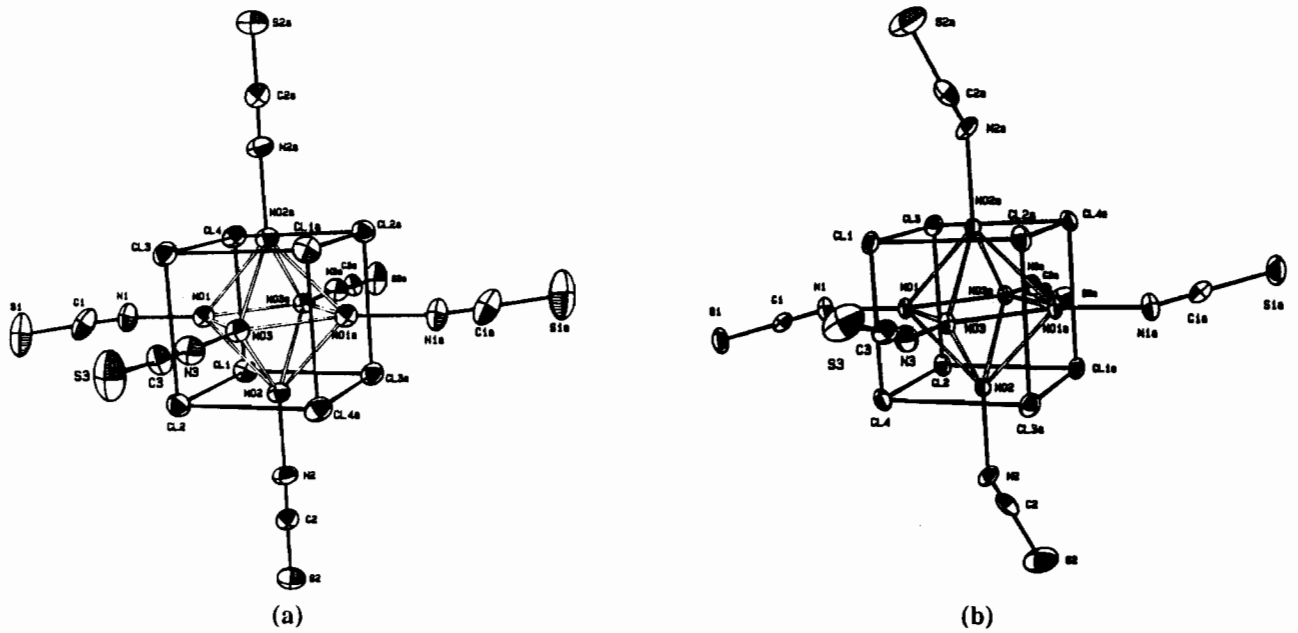

Figure 1. ORTEP views and atom labeling for the cluster anions in (a) $(Bu_4N)_2[Mo_6Cl_8(NCS)_6]$ (**1**) and (b) $[(MeS)_4TTF]_2[Mo_6Cl_8(NCS)_6]$ (**2**).

latter undergo terminal halide substitution to give a variety of substituted species.[14] The addition of a large excess (up to 60 equiv) of $Bu_4N(SCN)$ to an ethanol solution of $MoCl_2$ affords the substitution of most of the terminal chlorides. However, even under these conditions, total substitution proved difficult to achieve, and we preferred to proceed by first stripping off the outer labile halides by reaction with sodium hydroxide:

$$Mo_6Cl_{12} \xrightarrow[H_2O]{\text{6 equiv of NaOH}} 2Na^+,Mo_6Cl_8(OH)_6^{2-} \xrightarrow[MeOH]{HBF_4,\ Bu_4NNCS} (Bu_4N)_2Mo_6Cl_8(NCS)_6 \quad (1)$$

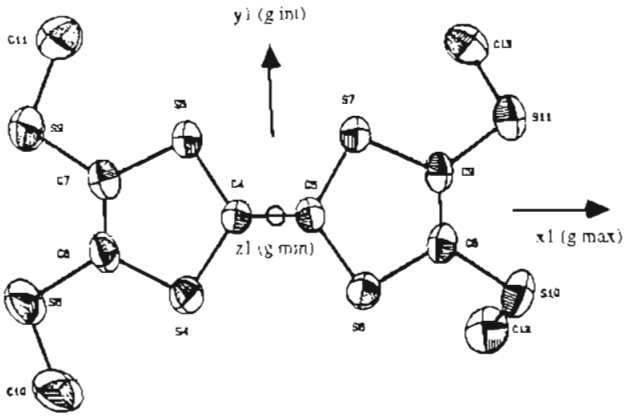

Figure 2. Atom labeling for the $(MeS)_4TTF$ molecule in **2** and **g** tensor molecular axis system (x_1, y_1, z_1).

Table IV. Selected Individual and Averaged Bond Lengths (Å) and Angles (deg) for $Mo_6Cl_8(NCS)_6^{2-}$ in **1** and **2**

	$(Bu_4N)_2$-$[Mo_6Cl_8(NCS)_6]$		$[(MeS)_4$-$TTF]_2$-$[Mo_6Cl_8(NCS)_6]$	
	individual value	averaged value	individual value	averaged value
Mo–N–C				
Mo1–N1–C1	159(1)		156.2(6)	
Mo2–N2–C2	177(1)		152(1)	
Mo3–N3–C3	177(1)		164.5(6)	
N–C–S		178(0)		177.5(5)
N1–C1–S1	178(1)		177.6(6)	
N2–C2–S2	178(1)		178(1)	
N3–C3–S3	178(1)		177.0(7)	
Mo–Mo		2.608(3)		2.608(2)
Mo–N		2.11(1)		2.16(4)
Mo1–N1	2.12(1)		2.124(5)	
Mo2–N2	2.09(1)		2.202(7)	
Mo3–N3	2.12(1)		2.149(6)	
N–C		1.14(3)		1.0(1)
N1–C1	1.11(1)		1.105(8)	
N2–C2	1.16(1)		0.895(9)	
N3–C3	1.14(1)		1.047(8)	
C–S		1.61(3)		1.7(1)
C1–S1	1.64(2)		1.636(7)	
C2–S2	1.60(1)		1.76(1)	
C3–S3	1.59(1)		1.641(8)	

Then, tetrafluoroboric acid was added to remove all six hydroxy groups, and the complexation of the thiocyanate ligands was favored rather than that of the tetrafluoroborate anions to yield **1**.

Structure of $(Bu_4N)_2[Mo_6Cl_8(NCS)_6]$. The cluster dianion is located at the origin of the monoclinic unit cell, and the tetrabutylammonium cation is in a general position. Note that while a large group of substituted species with the $\{Mo_6X_8\}$ core have been reported, few of their structures have been determined.[15] An ORTEP drawing of the molecular structure of $Mo_6Cl_8(NCS)_6^{2-}$ determined in **1** is given in Figure 1a. Within the hexathiocyanato-substituted Mo(II) halide cluster, the average Mo–Mo bond distance is 2.6070 Å, as expected.[7,10,15] The ligands act as linear isothiocyanates (Figure 1) with usual bond distances and angles (Table IV). In particular, the ∠Mo–N–C angles vary between 159 and 177°, which are typical coordinating angle values for isothiocyanate complexes whose geometry is not affected by steric constraints.[16]

Size and Shape of $Mo_6Cl_8(NCS)_6^{2-}$. The comparison in Figure 3 of the space-filling representations, at essentially identical orientation and scale, of $Mo_6Cl_8(NCS)_6^{2-}$ in **1** and $Mo_6Cl_8(Cl)_6^{2-}$,[17] emphasizes their striking differences in size and shape. Clearly, the former is less symmetrical and globular. In addition, given the unit-cell volumes of their tetrabutylammonium salts and the volumes[17] of Bu_4N^+ (443 Å^3) and $Mo_6Cl_{14}^{2-}$ (487 Å^3), one estimates that $Mo_6Cl_8(NCS)_6^{2-}$ is ca. 50% larger in volume (679 Å^3 vs 487 Å^3).

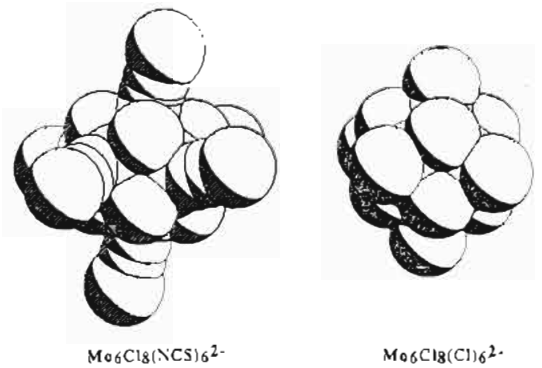

Figure 3. Compared space-filling (PLUTO) representations of $Mo_6Cl_8(NCS)_6^{2-}$ and $Mo_6Cl_8(Cl)_6^{2-}$.

Structure of $[(MeS)_4TTF]_2[Mo_6Cl_8(NCS)_6]$. Molecular Features. As exemplified in Figure 4, discrete organic dimer dications are interspersed between the functionalized cluster dianions in a CsCl-type structure similar to that of the parent salt $(Me_4TTF)_2Mo_6Cl_{14}$.[7]

It is of interest to note that, within the organic dimer, the molecules adopt the bond-over-ring pattern of intermolecular overlap associated with a fully slipped configuration (Figure 5). This, as well as the planarity of the inner TTF core of the donor molecules, is a characteristic feature of moderately coupled dimers as observed usually for such dimers inside mixed-valence, conducting stacks.[18] This contrasts with the configuration reported for such TTF salts with fully oxidized discrete dimers.[7] In particular, this is a distinctive feature of the molecular dication in the present salt when compared with $(Me_4TTF)_2Mo_6Cl_{14}$, for which strongly dimerized, diamagnetic dimers of distorted, eclipsed molecules are identified.[7]

Another remarkable feature is the observation (Figure 6) of smaller coordinating ∠MoNC angles for the isothiocyanate ligands and the Mo_6Cl_8 cluster core in **2** compared to those in the tetrabutylammonium salt, **1** (Table IV). This tends to indicate that increased intermolecular packing constraints are taking place in **2** while also demonstrating the conformational flexibility of the functionalized cluster anion in the latter structure.

Cation–Anion Binding. Three short intermolecular contacts between the organic and inorganic chalcogen atoms are identified in the structure, namely, S9···S1 = 3.793(3) Å, S11···S2 = 3.755(4) Å, and S10···S3 = 3.679(3) Å. In addition, each inorganic sulfur atom is engaged in at least one short C–H···S contact, with (C)H···S distances ranging from 2.861(4) to 3.009(3) Å and ∠CHS angles between 127.8(6) and 169.7(6)°. The latter, weakly attractive hydrogen bonds are directional and are effective at binding the molecular ions within their particular respective orientation.[19] The former chalcogen–chalcogen interactions are eventually rather repulsive and are likely to be involved in the organic–inorganic electronic coupling.

(15) (a) Guggenberger, L. J.; Sleight, A. W. *Inorg. Chem.* **1969**, *8*, 2041. (b) Healy, P. C.; Kepert, D. L.; Taylor, D.; White, A. H. *J. Chem. Soc., Dalton Trans.* **1973**, *646*. (c) Schäfer, H.; Brendel, C.; Henkel, G.; Krebs, B. *Z. Anorg. Allg. Chem.* **1982**, *491*, 275. (d) Chisholm, M. H.; Heppert, J. A.; Huffman, J. C. *Polyhedron* **1984**, *3*, 475. (e) Saito, T.; Nisida, M.; Yagamata, Y.; Ygamuchi, Y. *Inorg. Chem.* **1986**, *25*, 1111.

(16) See: Wells, A. F. *Structural Inorganic Chemistry*; Oxford University Press: Oxford, U.K., 1984; p 936.

(17) The anion geometry is taken from the structure of $(Bu_4N)_2Mo_6Cl_{14}$ which crystallizes in space group $P2_1/n$ with two formula units in a unit cell of volume 2746.4 Å^3: Boubekeur, K. Thesis, University of Rennes, 1989.

(18) See, for example, ref 6 and references therein.

(19) (a) Whangbo, M.-H.; Jung, D.; Ren, J.; Evain, M.; Novoa, J. J.; Mota, F.; Alvarez, S.; Williams, J. M.; Beno, M. A.; Kini, A. M.; Wang, H. H.; Ferraro, J. R. In *The Physics and Chemistry of Organic Superconductors*; Saito, G., Kagoshima, S., Eds.; Springer-Verlag: Berlin, 1990; p 262. (b) Novoa, J. J.; Whangbo, M.-H.; Williams, J. M. *Mol. Cryst. Liq. Cryst.* **1990**, *181*, 25. (c) Sarma, J. A. R. P.; Desiraju, G. R. *Acc. Chem. Res.* **1986**, *19*, 222. (d) Desiraju, G. R. *Acc. Chem. Res.* **1991**, *24*, 290.

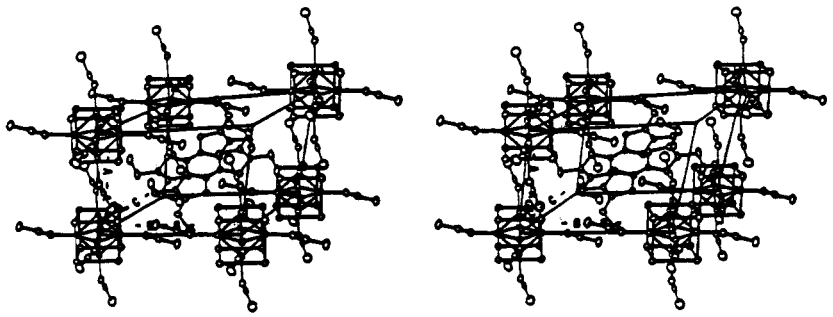

Figure 4. ORTEP stereoview of the unit cell of $[(MeS)_4TTF]_2[Mo_6Cl_8(NCS)_6]$ (**2**).

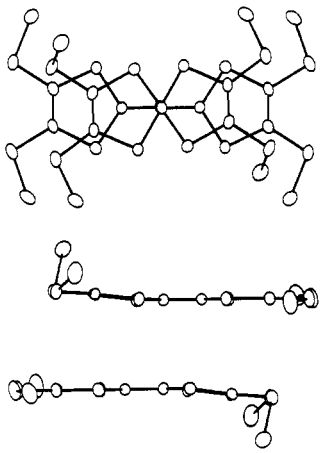

Figure 5. Two orthogonal projections (ORTEP) emphasizing the slipped configuration and the planarity of the $TTF^{\bullet+}$ inner cores within the $[(MeS)_4TTF]_2$ dimer in **2**.

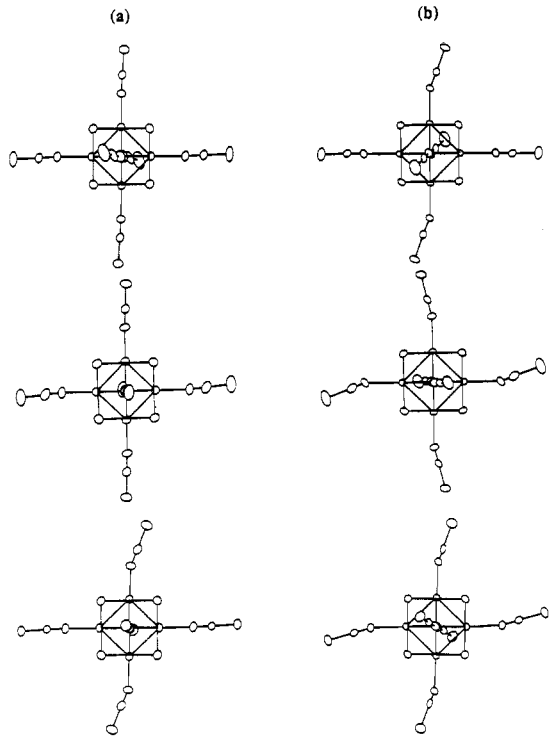

Figure 6. Compared geometries of the isocyanate ligand sets for the three independent projections of the octahedral cluster dianion core in (a) $(Bu_4N)_2[Mo_6Cl_8(NCS)_6]$ (**1**) and (b) $[(MeS)_4TTF]_2[Mo_6Cl_8(NCS)_6]$ (**2**).

ESR Spectra of $[(MeS)_4TTF]_2[Mo_6Cl_8(NCS)_6]$. A representative single-crystal ESR spectrum recorded at room temperature is shown in Figure 7. It consists of a central resonance, the so-called impurity line discussed in more detail below, and two lateral bands whose separation depends on the orientation of the crystal in the magnetic field. These features are characteristic of a triplet

Figure 7. Single-crystal ESR spectrum of $[(MeS)_4TTF]_2[Mo_6Cl_8(NCS)_6]$ at 22 °C.

exciton spectrum where the two symmetrical lateral bands are assigned to the two allowed $\Delta M_S = \pm 1$ transitions occurring within the $S = 1$ manifold and at two different fields separated by δH, a consequence of the zero-field splitting (ZFS). There is only one magnetic site in the structure, namely, the dimer of the moderately coupled cation radicals $[(MeS)_4TTF^{\bullet+}]_2$. Thus, the zero-field splitting originates in the dipolar interaction between the two unpaired electron spins within the dimer. Note that a largely dissymmetrical spin distribution within the dimer framework will result in a large value of the ZFS and a significant anisotropy of δH as well.

Determination of *D* and *E*, the ZFS Parameters. Since the orientation of the molecular (dimer) axis system (x_1, y_1, z_1) with respect to the crystal morphology was unknown, we proceeded in the following manner. First, the variations of δH were determined at room temperature by rotating the platelet single crystal around three orthogonal axes x, y, and z. Thus, the orientation of the fine structure tensor in the (x, y, z) reference system was determined as well as the magnitude of its principal values. The g values were also determined for each of those orientations, hence affording the orientation of the **g** tensor in the (x, y, z) system. Now, given Walsh classical results[20] on the orientation and relative magnitude of the tetrathiafulvalenium **g** tensor within the molecular framework (x_1, y_1, z_1) (Figure 2), the fine structure tensor orientation within the same molecular axis system is readily obtained (Table V).

For the remainder of the discussion, the commonly used fine structure parameters D and E are obtained from the experimental determination of the ZFS tensor principal values d_{XX}, d_{YY}, and d_{ZZ}, as follows:

$$D = \frac{3}{2}d_{ZZ} \qquad E = \frac{1}{2}(d_{XX} - d_{YY}) \tag{2}$$

Note that the sign of ZFS parameters was attributed relatively to the attractive or repulsive nature of the interaction expected to be found in the direction of the different fine structure principal axes.

(20) Walsh, W. M., Jr.; Rupp, L. W., Jr.; Wudl, F.; Kaplan, M. L.; Schafer, D. E.; Thomas, G. A.; Gemmer, R. *Solid State Commun.* **1980**, *33*, 413.

Table V. Experimental and Calculated Fine Structure Tensors for **2** at 22 °C

principal values, G	ZFS params, G	principal direction cosines in the molecular axis system (x_1, y_1, z_1) principal axis	x_1	y_1	z_1
Experimental Values					
$D_{XX} = 70$	$D = -315$	X	0.84	0.39	−0.37
$D_{YY} = 140$	$E = 35$	Y	−0.42	0.91	0.02
$D_{ZZ} = -210$	$D/E = -9.0$	Z	0.35	0.14	0.93
Calculated Values					
$D_{Xc} = 143$	$D_c = -567$	X_c	0.9681	−0.0045	−0.2507
$D_{Yc} = 235$	$E_c = 46$	Y_c	0.0034	0.9999	−0.0047
$D_{Zc} = -378$	$D_c/E_c = -12.3$	Z_c	0.2507	0.0037	0.0968

Singlet–Triplet Energy Separation. The intensity of one of the symmetrical lateral bands was measured between 295 and 197 K, using the product of height and the square of the line width. Note however that the line width maintains a constant value throughout the entire temperature range. In the case of an activated triplet state, the intensity of the ESR absorption is given by[5]

$$I \propto \frac{1}{T}\left[\exp\left(\frac{J}{kT}\right) + 3\right]^{-1} \tag{3}$$

where J is the magnetic gap. For the usual situation where $J \gg kT$, the latter reads

$$I \propto \frac{1}{T}\exp\left(\frac{-J}{kT}\right) \tag{4}$$

as verified experimentally (Figure 8), giving a singlet–triplet energy gap $J = 0.215$ eV.

On the basis of the Hubbard Hamiltonian for noninteracting dimers,[21] the magnetic gap reads

$$\Delta = \frac{1}{2}\sqrt{U_{\text{eff}}^2 + 16t^2} - \frac{U_{\text{eff}}}{2} \tag{5}$$

with U_{eff} being the effective on-site repulsion for two electrons (ca. 1.0 eV[22]) and $t = 0.253$ eV being the intradimer transfer integral obtained by extended Hückel calculations[23] for the present dimer geometry. Given these parameters, the calculated magnetic gap amounts to $\Delta = 0.211$ eV, a value in excellent agreement with experiment and typical of moderately coupled systems (Table I). In this respect, in the case of $TTF{\cdot}I_3$, where discrete, strongly dimerized eclipsed dimers are identified, the calculated magnetic gap reaches 0.763 eV.

Thus, these results point to a direct relationship between the configuration of the dimer and the occurrence of triplet-state activation. Indeed, a moderate value of the magnetic gap is required in the latter case and is associated with a slipped configuration of planar molecular cation radicals as in **2** and $[(TTF^{\bullet+})_2](Nb_6Cl_{18}^{3-})[(C_2H_9)_4N^+](CH_3CN)$.[6] Conversely, large values of the magnetic gap occur with ESR-silent dimers, which all present an eclipsed pattern of overlap of strongly distorted molecular ions as exemplified by $(Me_4TTF)_2Mo_6Cl_{14}$ and $TTF{\cdot}I_3$.

Assuming that the slipping of the cation radical molecules within the dimer will affect primarily the transfer integral t with only minor changes in U_{eff}, then the structure–magnetic activation correlation described above can be rationalized in simple terms. Thus, the stronger the intradimer overlap, the larger the stabilization of the $S = 0$ state. Clearly, the totally eclipsed intradimer configuration optimizes the overlap while the latter increasingly weakens upon a slipping of the molecular cation radicals. As observed previously,[24] the minimum intradimer overlap is achieved for an offset of ca. 1.6 Å, the typical slipped configuration identified in the triplet active systems, which indeed corresponds to the minimum activation energy for the triplet state.

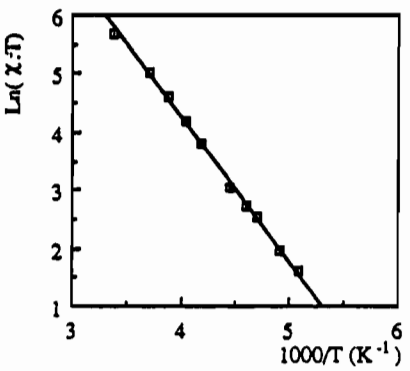

Figure 8. Temperature dependence of the integrated ESR intensity of the triplet-state resonance.

Analysis of the Central Impurity Resonance. A central, complex impurity resonance was observed for each sample regardless of the conditions of preparation. Note that the line centered at $g \approx 2.00$ was present for every sample, albeit with variable intensities, while the smaller (Figure 7) line was not observed for other samples from different batches. These impurity features have already been observed for other excitonic systems as thoroughly discussed previously.[5] The temperature dependence of the central line was determined (Figure 9). In a high-temperature regime an activated susceptibility was observed with an activation energy of 0.117 eV, that is, essentially half of the singlet–triplet energy separation, as observed earlier.[2,5d,g]

The Calculated Fine Structure Tensor. It is of interest to compare the fine structure tensor parameters D and E and the tensor orientation, determined previously from experiment, with the corresponding calculated values[25] and orientation. This requires the knowledge of the spin densities on each of the dimer atoms since the fine structure tensor elements are given (Appendix I, supplementary material) by[26]

$$d_{\alpha\beta} = \frac{1}{2}g_e^2\beta^2 \sum_{i\in R_1, j\in R_2} \rho_i\rho_j\left(\frac{\delta_{\alpha\beta}}{r_{ij}^3} - \frac{3r_{ij}^{\alpha}r_{ij}^{\beta}}{r_{ij}^5}\right) \tag{6}$$

where R_1 and R_2 stand for $[(MeS)_4TTF^{\bullet+}]_1$ and $[(MeS)_4TTF^{\bullet+}]_2$ and ρ_i (ρ_j) stands for the spin density of electron 1 (2) on atom i (j) within R_1 (R_2).

The atomic spin densities were obtained by extended Hückel calculations performed on the crystal structure dimer geometry.

The calculated fine structure parameters D_c and E_c and the corresponding principal values and tensor orientation are given in Table V. The scaling factor relating the experimental δH tensor to the theoretical fine structure tensor $d_{\alpha\beta}$ is expressed in Appendix II (supplementary material).

Discussion

The Structure–Electronic Properties Relationship. The Fine Structure Tensor Orientation. At the onset of this discussion, it is of interest to observe that the fine structure tensor principal

(21) (a) Hubbard, J. *Proc. R. Soc. London* **1963**, *A276*, 238. (b) Harris, A. B.; Lange, R. V. *Phys. Rev.* **1967**, *157*, 295.
(22) Mazumdar, S.; Dixit, S. N. *Phys. Rev. B* **1986**, *34*, 3683.
(23) (a) EH calculations yield the HOMO–LUMO gap for the $[(MeS)_4(TTF^+)_2]$ dimer, which corresponds to $2t$, as in the MO approach. The calculations were carried out using single-ζ type orbitals. Given the observation that the overlap in **2** is similar to that in TTF-TCNQ, it seems reasonable to use the results found for the latter compound, that is $t_{\text{exp}} = 1.366t_{\text{single-}\zeta}$[23b,c] to normalize those for the dimer, which leads to $t_{\text{exp}} = 0.253$ eV. (b) Cowan, D. O.; Mays, M. D.; Kistenmacher, T. J.; Poehler, T. O.; Beno, M. A.; Kini, A. M.; Williams, J. M.; Kwok, Y.; Carlson, K. D.; Xiao, L.; Novoa, J. J.; Whangbo, M.-H. *Mol. Cryst. Liq. Cryst.* **1990**, *181*, 43. (c) Jacobsen, C. S. *Mat.-Fys. Medd.—K. Dan. Vidensk. Selsk.* **1985**, *41*, 251.
(24) Lowe, J. P. *J. Am. Chem. Soc.* **1980**, *102*, 1262.
(25) We warmly thank Marc Couty for programming the calculation of $d_{\alpha\beta}$.
(26) Attherton, N. M. *Electron Spin Resonnance*; Ellis Horwood: Chichester, U.K., 1973; p 155.

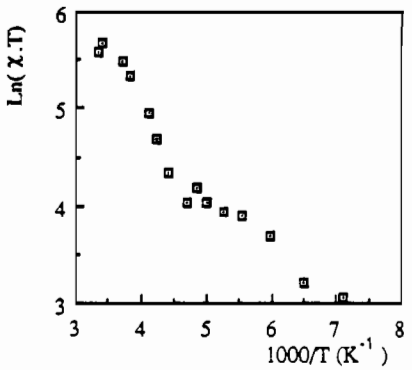

Figure 9. Temperature dependence of the integrated ESR intensity of the impurity resonance.

Chart I

eclipsed configuration slipped configuration

axis system, as determined in the experiment, essentially matches the molecular symmetry of the cation radicals (Table V) and that of their dimer. In other words, the observed macroscopic triplet exciton serves as a probe of the electronic and molecular structure of the active magnetic species and its environment.[27]

There is a fair agreement between the experimental and calculated principal axis coordinates of the fine structure tensor (Table V). Note however that, if one takes as a reference the symmetry axes of the central TTF core, that is the *g* factor tensor principal axis system (x_1, y_1, z_1) as shown in Figure 2, there is a striking offset of the Y component of the fine structure tensor determined experimentally. Indeed Y is rotated by 24.5° off the molecular symmetry axis y_1 whereas its calculated corresponding component Y_c precisely matches y_1. This latter result is simply the straightforward consequence of calculations performed on a dimer of planar molecular cations offset along x_1 only and bearing a spin density symmetrical with respect to x_1, as discussed in more detail in Appendix III (supplementary material). The observed mismatch between Y and y_1 demonstrates however that the actual spin density is likely to be less symmetrical than assumed in the calculation. Therefore, an asymmetric spin distribution occurs within the dimer in the solid state as detected by the present comparison of the observed and calculated principal axes (X, Y, Z) of the triplet state. We believe that this perturbation of the molecular spin densities in the solid state are induced by the asymmetric binding of the outer methylthio and thiocyanate functionalities, as discussed earlier in the analysis of the crystal structure of **2**. This demonstrates the sensitivity of the fine structure splitting to the molecular environment and the efficiency of ESR experiments in finding spin distributions in ion radical crystals.[27]

Likewise, one identifies a 21.5° offset between Z and z_1 (Table V). Clearly, this offset angle is essentially accounted for by the slipped pattern of intermolecular overlap within the dimer. Indeed, a simple geometrical argument, sketched in Chart I, predicts an offset angle $\theta = 22°$ for the lateral offset $\delta = 1.35$ Å and intradimer separation $d = 3.25$ Å, determined for the structure. Thus, there is a simple correlation between the dimer configuration and the easy axis for dipolar interaction, Z.

ZFS Parameters. The experimental values obtained for D and E (Table V) are comparable to those ($D = 474$ G) reported by Grossel et al. for Rb^+(18-crown-6)$TCNQ^-$, where the triplet exciton is localized in quasi-isolated dimers.[2a,c] It is significantly larger than the values reported ($D = 40$–150 G) for stacks of TCNQ radical anions.[5]

The calculated D and E values are largely overestimated when compared to the experimental results, a common, recurrent observation in the study of excitonic systems.[5] There is no possibility in **2** for sharing of the triplet exciton[28] since the discrete dimers are isolated in the inorganic cluster framework and, therefore, the observed discrepancy may be ascribed[29] to inadequacies of the point-dipole approximation.

Finally, it should be pointed out that comparatively small variations of the set of atomic spin densities will affect significantly the magnitude of the ZFS parameters which are proportional to r^{-3} (eq 6), with no effect on the tensor orientation itself. Thus, even a slight increase in the spin density at the outer sulfur atoms would reduce the calculated values of D and E, implying that the actual spin density is likely to be shifted over to the outskirt of the molecules. This further supports the former assumption of an outer functionality-mediated environment effect.

Mobile Frenkel Excitons and the Outer Chalcogen Interaction. No hyperfine structure is detected in Figure 7, which demonstrates that the coupling between the electronic and nuclear spins is averaged in **2** by the rapid motion of the triplet spin excitons, hence the observed motional narrowing of the absorption line. This absence of hyperfine structure is common in TCNQ salts exhibiting triplet excitons and is a consequence of the easy migration of the triplet excitation along the stacks.[5a] In **2** however, the dimers are isolated from each other and it is suggested that the exciton mobility may only be explained if one takes into account a superexchange mechanism of the triplet excitation across the inorganic cluster anions. This supplements the crystal structure analysis indications that the particular binding of the outer organic–inorganic chalcogen atoms may affect the electronic properties of this solid.

Finally, the observation of a fine structure in the triplet state resonance of **2** indicates, as elegantly expressed in Soos' classical paper,[1] that the unpaired electrons in the triplet state remain adjacent and form a Frenkel, or strongly correlated, spin excitation. Thus, in chemical terms, there is a correlation between the fine structure tensor principal axes and the dimer molecular axes,[2] as thoroughly analyzed in this paper.

Acknowledgment. Financial support by the CNRS and discussions with Enric Canadell are gratefully acknowledged.

Supplementary Material Available: Tables giving atomic coordinates, bond lengths, bond angles, anisotropic thermal parameters, hydrogen atom locations, and the least-squares plane of the TTF core, formulation of the dipolar Hamiltonian (Appendix I), analytical correspondence between the experimental doublet splitting tensor δH and the fine structure tensor (Appendix II), and derivation of the analytical expression for the fine structure tensor of the slipped dimer in the hypothetical case of a symmetrical spin distribution (Appendix III) (18 pages). Ordering information is given on any current masthead page.

(27) Silverstein, A. J.; Soos, Z. S. *Chem. Phys. Lett.* **1976**, *39*, 525.

(28) Hibma, T.; Dupuis, P.; Kommandeur, J. *Chem. Phys. Lett.* **1972**, *15*, 17.

(29) The validity of the atomic spin densities calculated under the EH formalism may also be questioned. Note however that our calculated spin densities compare very well with those calculated by SCF methods for TTF^+: Kinoshita, N.; Tokumoto, M.; Anzai, H.; Ishiguro, T.; Yamabe, T.; Teramae, H.; Saito, G. *Mol. Cryst. Liq. Cryst.* **1985**, *119*, 221.